



## A comparative experimental study of two multi-robot olfaction methods: Towards locating time-varying indoor pollutant sources

Mingrui Jiang<sup>a</sup>, Yu Liao<sup>a</sup>, Xun Guo<sup>a</sup>, Hao Cai<sup>a,\*</sup>, Wenqing Jiang<sup>c</sup>, Zhou Yang<sup>d</sup>, Fei Li<sup>a</sup>, Fei Liu<sup>b</sup>

<sup>a</sup> Department of HVAC, College of Urban Construction, Nanjing Tech University, Nanjing, 210009, PR China

<sup>b</sup> Defense Engineering Institute AMS, PLA, Beijing, 100036, PR China

<sup>c</sup> School of Information Science & Technology, Shanghai Tech University, Shanghai, 201210, PR China

<sup>d</sup> Plasma Propulsion Lab, Institute of Advanced Power, Harbin Institute of Technology, Harbin, 150001, PR China



### ARTICLE INFO

#### Keywords:

Indoor environment  
Time-varying source  
Mobile robot olfaction  
Source localization  
Experimental validation

### ABSTRACT

Locating the source of indoor pollutants/hazardous substances is essential to ensure the health and safety of indoor personnel. The existing studies on source localization using robots rarely focus on time-varying sources whose release rate changes with time. However, in practical applications, time-varying sources are ubiquitous, and it is usually more difficult to locate a time-varying source than a constant source with a constant release rate. This study aims to locate time-varying sources in a real-world indoor environment by using our two newly proposed two multi-robot olfaction methods, namely, the improved particle swarm optimization (IPSO) method and the improved whale swarm algorithm (IWOA) method. To this end, we developed a source localization system composed of three robots and compiled the IPSO and IWOA methods into executable programs. This study conducted 160 experiments for four scenarios, which included two time-varying source types (periodic source and decaying source) and two source locations. In each scenario, 20 independent experiments were conducted for each method. For all four scenarios, the mean success rates of the IPSO and IWOA methods were 80% and 91%, respectively, indicating that both methods have the potential to locate indoor time-varying sources. In terms of the success rate, locating efficiency and locating accuracy, the overall performance of the IWOA method was better than that of the IPSO method. The advantages of the IWOA method were its success rate and locating accuracy, while the disadvantage was its locating efficiency.

### 1. Introduction

The health and safety of people indoors depend on the effective control of indoor airborne pollutants or hazardous substances. Common control measures such as source control, pollutant isolation, ventilation, and air purification normally require first locating the pollution/hazard source, which has motivated research on indoor source localization [1–4]. The dispersion of pollutants or hazardous substances in indoor airflow is directly affected by the temporal profile of the source, according to which indoor sources can roughly be divided into three categories: instantaneous sources that are suddenly released in a short time interval, constant sources that are continuously released at a constant rate, and time-varying sources that are released at a variable rate during a certain period of time [5,6].

This study focuses on locating time-varying sources in mechanically ventilated indoor environments for three main reasons. First, the

locating of time-varying sources, typically periodic sources and decaying sources, covers a wide range of real-world needs, including identifying asymptomatic infected persons in public places during a pandemic such as the recent COVID-19 pandemic [7], optimizing demand-controlled ventilation according to the CO<sub>2</sub> distribution [8], locating hazardous gas leaks in industrial plants [9,10], and even more extreme, finding deliberate releases in biochemical terrorist attacks [11, 12]. Second, instantaneous sources and constant sources are just special cases of time-varying sources in theory. Third, compared with the extensive research on locating indoor instantaneous and constant sources [13–17], the research on locating indoor time-varying sources is still lacking [18,19].

One category of source localization method is called the stationary sensor network (SSN) method, which typically uses the readings of one or more sensors installed in the building space and combines them with the forward or inverse solution of the pollutant transport models (e.g.,

\* Corresponding author.

E-mail address: [caihao@njtech.edu.cn](mailto:caihao@njtech.edu.cn) (H. Cai).

computational fluid dynamics (CFD) or multi-zone model) to identify indoor pollution sources [20]. SSN research was initiated to identify indoor instantaneous and constant sources. At present, extensive research has been conducted, and substantial progress has been made. Typical SSN methods include the quasi-reversibility and pseudo-reversibility methods [21–23], the regularization method [18, 24], the probability-based adjoint inverse modeling method [20, 25], the Markov-chain-based inverse modeling method [2, 26], the optimization-based methods [13, 27, 28], and the Bayesian probability methods [29, 30].

In recent years, SSN research has made encouraging progress in identifying indoor time-varying sources. For example, Zhang and co-workers [18] proposed an inverse method based on Tikhonov regularization and least-squares optimization for identifying a sinusoidal source. They further improved this method and tested it for locating a single [31] and multiple periodic sources [19] through CFD simulations. Zhai et al. [5] proposed a dynamic standard adjoint location probability method to identify a single source with a randomly changing release rate and validated this method with experimental measurements. Although encouraging progress has been made, the SSN methods still face at least one of the following limitations in real-world applications: (1) sensors for target gases should be deployed in advance; (2) sufficient information on the building space should be known to build a simulation model in advance; (3) the simulation results should be sufficiently accurate; and (4) the boundary conditions (e.g., speed and direction of the supply air) should be obtained in advance or in real time. In general, how to adapt to more complex, uncertain, or even unknown real-world scenarios will be the major challenge for future SSN research.

Another category of source localization method is called the mobile robot olfaction (MRO) method, which uses a single or multiple robots to actively find a target gas, track the gas plume, and finally approach and confirm the source [32]. Compared with stationary sensors, mobile robots can be deployed quickly when an event occurs, explore unfamiliar indoor areas, and adapt to environmental changes and can be extended to perform versatile functions, such as routine inspections, source control, and leakage disposal [33]. MRO methods usually do not require solving an indoor pollution dispersion model and can be applied to environments with uncertain boundary conditions or even unknown environments.

To date, most MRO studies for indoor environments have focused on locating constant sources [14, 34, 35], while there have been few attempts to locate time-varying sources [36]. Due to the chaotic effect of indoor turbulence, the pollutant from a constant source will be dispersed as a meandering and patchy plume, and the concentration at a certain point in the space will fluctuate intermittently [37]. If the effect of the time-varying release rate is coupled, there will be irregular overlaps of multiple plumes of different structures in space and time. In addition, due to the superposition of the concentration fluctuation caused by turbulence and the concentration changes due to time-varying sources, the overall concentration fluctuation at a certain point in space can be sharper and more irregular.

Due to the influence of time-varying sources on the spatio-temporal distribution of a concentration, the robots used for source localization will face greater challenges, such as the following: (1) a more complex spatio-temporal distribution of a pollutant will make it more difficult for robots to continuously track a stable plume; (2) the sharper and more irregular concentration fluctuations will cause more elusive changes in the direction of the concentration gradient, which will cause the robots to deviate from the correct direction of travel; and (3) the spatial and temporal superposition of the concentration in areas without a source may produce more local extremum areas, that is, areas where the concentrations are higher than those in the surrounding areas. These local extremum areas will act like traps preventing each robot from approaching the true source.

To overcome the above challenges, our research team has conducted several numerical studies on the use of the MRO methods to locate

indoor time-varying sources [36, 38–40]. Chen et al. [38] presented and validated a particle swarm optimization (PSO)-based method for locating decaying sources in a CFD-simulated 2D indoor environment. This method was extended to 3D by Feng et al. [36, 39] and validated in various 3D indoor environments simulated by CFD. Inspired by the success of the emerging whale optimization algorithm (WOA) in the field of optimization, Yang et al. [40] developed a standard WOA (SWOA) method and an improved WOA (IWOA) method for locating time-varying indoor particle sources without and with airflow information, respectively. Through a total of 3200 experiments in CFD-simulated 3D indoor environments, this study showed that the SWOA and IWOA methods are effective and generally outperform the standard PSO (SPSO) and the improved PSO (IPSO) methods in locating decaying and periodic sources.

Although our previous studies have shown the potential of the MRO methods to locate indoor time-varying sources, the CFD-simulated environments in these studies cannot fully reproduce the difficulties that robots may encounter in real-world environments. First, in the time-averaged CFD outputs, although the concentration changes due to the time-varying source can be observed, the intermittent fluctuations in an instantaneous concentration due to the chaotic turbulence effect cannot be found. Second, the numerical studies did not consider the sensor characteristics, such as the response/recovery time and measurement errors. In addition, the numerical studies did not consider the actual performance of the robots, such as the collisions between robots and the interference of the robots with the environment.

This study aims to experimentally validate and compare the two methods that showed the potential for locating time-varying sources in our previous numerical studies, namely, the IPSO and IWOA methods. To this end, we developed an MRO system composed of three mobile robots and designed 8 experimental scenarios involving a combination of the two MRO methods (IPSO and IWOA), two typical time-varying sources (periodic source and decaying source), and two source locations (DS: source location in the downwind zone, and RS: source location in the recirculation zone). To obtain statistically significant results, each scenario was tested via 20 independent experiments, and a total of 160 experiments were conducted. The main contributions of this study lie in the experimental validation of the IPSO and IWOA methods, the comparison of their performance, and the analysis of their influencing factors. All these not only make up for the deficiencies of numerical research, but also promote the above methods from theoretical research to practical application.

## 2. Source localization method

### 2.1. Overview of the two source localization methods

Both the IPSO and IWOA methods locate the source through three basic movement modes: plume-finding mode, plume-tracking mode, and source-confirming mode. Here, the plume refers to a feather-like trajectory formed when the source released and dispersed in the air [41]. It is a medium for the robots to locate the source. As shown in Fig. 1, in the plume-finding mode, multiple robots start from the starting positions and implement the divergence search algorithm to find the plume. When any robot detects a concentration above a preset threshold  $C_{\min}$ , all robots switch to the plume-tracking mode and use the IPSO or IWOA algorithm to continuously track the plume. This mode continues until the robots determine that they have become trapped in a local extremum area (an area in which the concentration level is higher than that in the surrounding area), at which point the robots switch to the source-confirming mode to determine whether they have found the actual source. If the actual source has been found, the robots will terminate the source localization task and report the source location. Otherwise, the robots will start the plume-finding algorithm to escape the current local extremum area. If the robots determine that they have been escaped the local extremum area, they will try to rediscover the

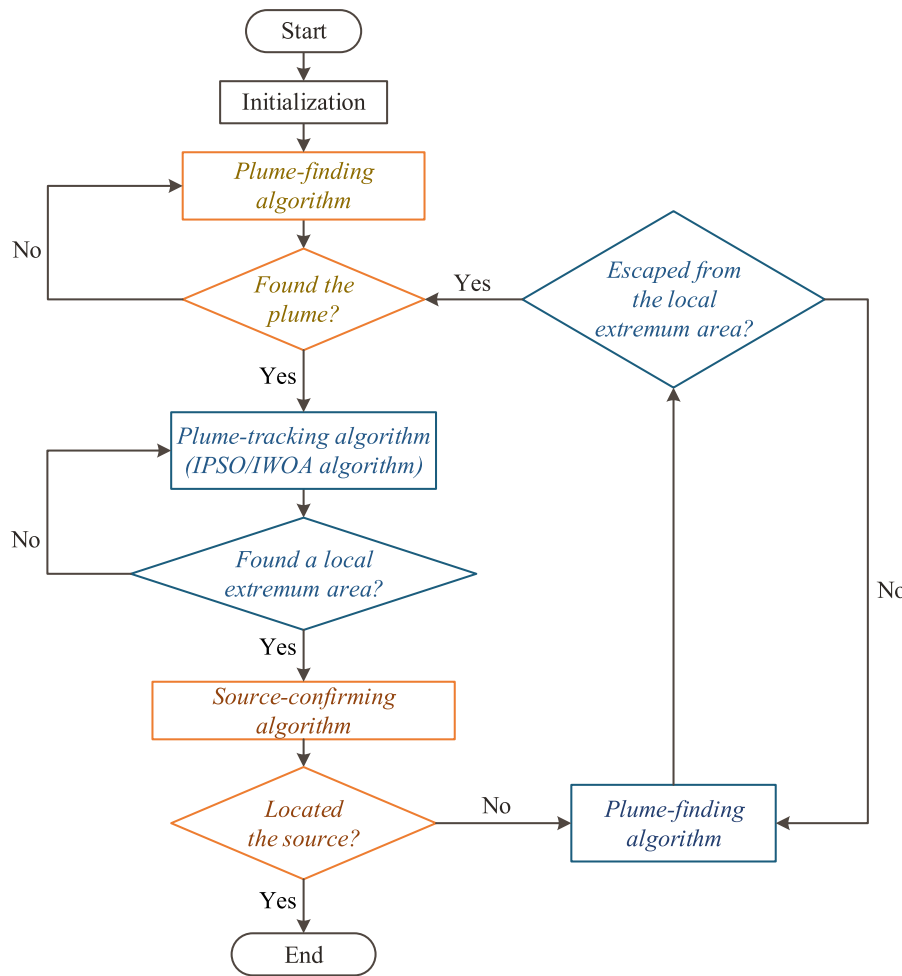


**Fig. 1.** Flow chart of the IPSO and IWOA methods for source localization.

plume and continue to track the plume until they enter a local extremum area again. For a more detailed description of the source localization methods, please refer to our previous paper [42].

In the field of MRO, there is a consensus that the plume-tracking algorithm is the core part of the source localization method [43], and the plume-tracking algorithm is the most considered and most extensively studied [4,44]. The reason why the plume-tracking algorithm is so important may be that in practical applications, robots are often required to approach the source by continuously tracking the plume from far away. To focus on the performance of the source localization method in tracking the plume and to ensure the fairness of the comparison, the IPSO and IWOA methods use only different algorithms in the plume-tracking mode.

## 2.2. Algorithm of the plume-finding mode

In the plume-finding mode, the robots use a divergent search algorithm to find the plume and expand the scope of exploration. As shown in Fig. 2 (a), all robots start at the same time from their initial positions (SP1–SP3) and move at the same speed. The trajectory of each robot is a straight line, and the angles between these trajectories are the same. Once a robot detects the target pollutant, all robots switch to the plume-tracking mode (Fig. 2 (b)).

## 2.3. Algorithms of the plume-tracking mode

In the following, we briefly introduce the IPSO and IWOA algorithms. For more details, please refer to our previous research [36,40].

### 2.3.1. IPSO algorithm

The PSO algorithm is a stochastic optimization technique inspired by the behaviors of bird and fish swarms in situations involving, e.g., the search for food and escaping danger [45]. Compared with other swarm intelligence algorithms, the PSO algorithm is easy to apply, offers fast convergence, involves few parameters, and has low computational complexity. To date, the PSO algorithm has been widely used in the communications, biology, control, military and security fields [45].

Using the SPSO algorithm, the robots depend only on the concentration information to update their positions during the plume-tracking process; however, this causes the robots to be prone to falling into local extremum areas. To solve this problem, the IPSO algorithm was proposed in our previous study, which introduces an upwind term that allows the robots to use the airflow information to correct their positions at the next time step [42,46].

### 2.3.2. IWOA algorithm

The WOA algorithm is a nature-inspired metaheuristic optimization algorithm recently proposed by Mirjalili and Levisa in 2016 that mimics the hunting behavior of humpback whales [47]. This algorithm has been tested on 29 mathematical optimization problems and 6 structural design problems, and the results have shown its competitiveness compared to the state-of-the-art metaheuristic algorithms as well as conventional methods.

The WOA algorithm mimics the three behavior patterns of humpback whale groups, namely, encircling prey, bubble-net attacking and searching for prey. Corresponding to these three patterns, the WOA algorithm includes three mechanisms: the contraction mechanism, the

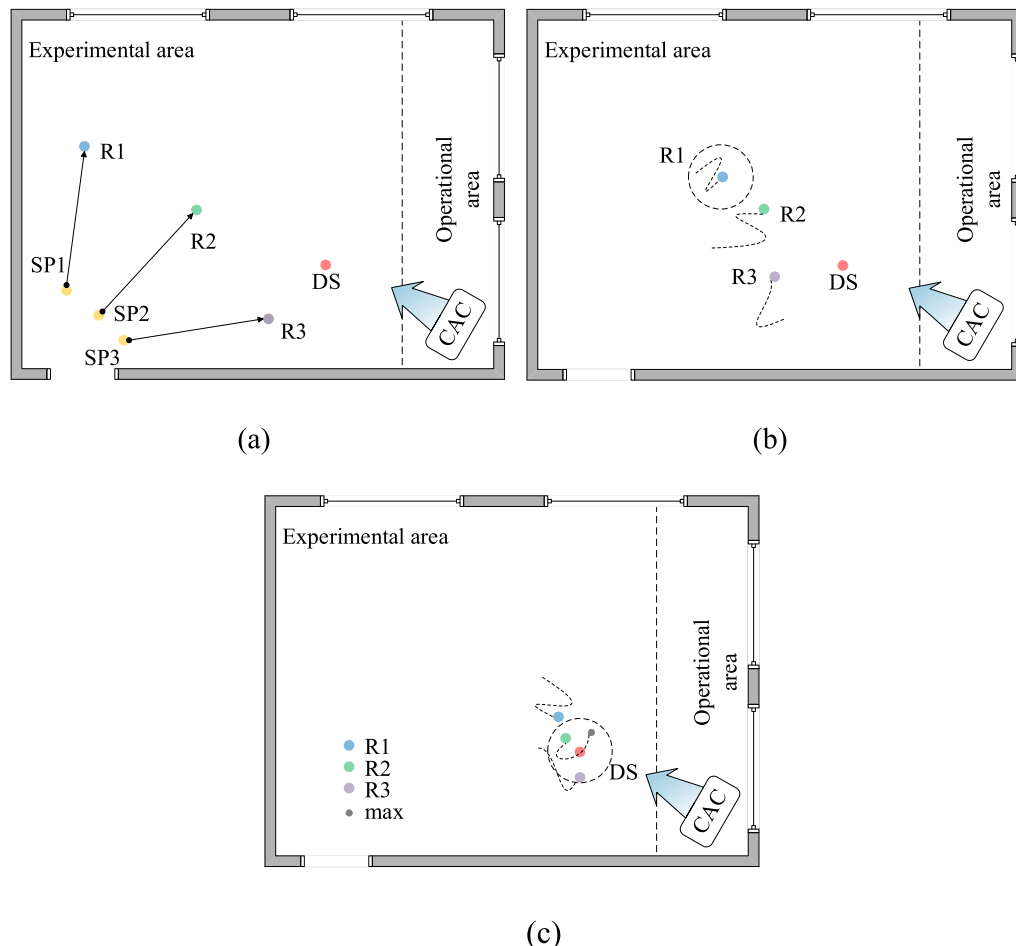


**Fig. 2.** Schematic diagram of the three basic movement modes: (a) plume-finding; (b) plume-tracking; (c) source-confirming (DS: source location in the downwind zone; R1–R3: robots; SP1–SP3: starting positions of the robots; max: global optimal position; CAC: cabinet air conditioner).

spiral renewal position mechanism and the random hunting mechanism.

#### (1) Contraction mechanism

The contraction mechanism corresponds to the “encircling prey” behavior of a humpback whale group. For the source localization problem, the source can be regarded as the prey. The WOA algorithm assumes that the robot with the highest concentration detected is currently at the best robot position and that other robots will approach the best robot position according to the following equations:

$$\vec{D} = \left| \vec{C} \cdot \vec{X}^*(t) - \vec{X}(t) \right| \quad (1)$$

$$\vec{X}(t+1) = \vec{X}^*(t) - \vec{A} \cdot \vec{D} \quad (2)$$

where  $t$  is the current time step;  $\vec{X}^*$  is the best robot position, which is first updated after starting a new search;  $\vec{X}$  is the robot position to be updated;  $\vec{C}$  is a coefficient vector that is linearly decreased from 2 to 0;  $\vec{D}$  indicates the random distance between the best robot position and the current robot position; and  $\vec{A}$  is a random coefficient vector in  $[-1, 1]$ .

#### (2) Spiral renewal position mechanism

Corresponding to the “bubble-net attacking” behavior, the spiral renewal position mechanism includes two position update strategies:

shrinking encircling and spiral updating. In practice, these two strategies are implemented simultaneously; thus, the probability of each strategy is 50%, as described by the following equation:

$$\vec{X}(t+1) = \begin{cases} \vec{X}^*(t) - \vec{A} \cdot \vec{D} & p < 0.5 \\ \vec{D} \cdot e^{bl} \cdot \cos(2\pi l) + \vec{X}^*(t) & p \geq 0.5 \end{cases} \quad (3)$$

where  $\vec{D}$  is the distance between  $\vec{X}^*(t)$  and  $\vec{X}(t)$ ;  $b$  is a constant that defines the shape of the logarithmic spiral; and  $l$  and  $p$  are two random numbers in  $[-1, 1]$  and  $[0, 1]$ , respectively.

#### (3) Random hunting mechanism

By imitating the “searching for prey” behavior, the random hunting mechanism determines whether to hunt randomly according to the value of  $\vec{A}$ . If  $|\vec{A}| > 1$ , the robots will move away from a randomly selected reference robot, as described by the following equation:

$$\vec{D} = \left| \vec{C} \cdot \vec{X}_{rand}(t) - \vec{X}(t) \right| \quad (4)$$

$$\vec{X}(t+1) = \vec{X}_{rand}(t) - \vec{A} \cdot \vec{D} \quad (5)$$

where  $\vec{X}_{rand}$  is the position of the randomly selected reference robot.

In our previous research, we added an upwind term to the WOA algorithm to enhance the ability of robots to track the plume by intro-

ducing airflow information [48]. The correction of the movement of the robot by the airflow information is described by the following equations:

$$\vec{X}(t+1) = \alpha \vec{X}_{wind}(t) + \vec{X}(t) \quad (6)$$

$$\vec{X}_{wind}(t) = \begin{cases} -L_{\max} \times \vec{V}^s(t) / |\vec{V}^s(t)| & \text{if } |\vec{V}^s(t)| \geq V_{\min}^s \\ L_{\max} \times \vec{V}_r & \text{if } |\vec{V}^s(t)| < V_{\min}^s \end{cases} \quad (7)$$

where  $\vec{X}_{wind}(t)$  is the unwind term at time  $t$ ;  $\alpha$  is a random number in  $[0, 1]$ ;  $L_{\max}$  is the maximum step length of the robots;  $\vec{V}^s(t)$  is the airflow velocity vector;  $V_{\min}^s$  is the threshold of the anemometer; and  $\vec{V}_r$  is a random vector uniformly distributed in  $[-1, 1]$  [36].

#### 2.4. Algorithm of the source-confirming mode

In the plume-tracking process, the maximum value of the concentration detected by all robots up to the current moment is called the global optimal value, and the position where the maximum value was detected is called the global optimal position. If the change in the global optimal position in a preset time period  $\Delta T$  is less than a preset distance  $d_{\min}$ , the robots will conclude that they have fallen into a local extremum area and then switch to the source-confirming mode.

In the source-confirming mode, the robots determine whether the real source is found according to the global optimal value. If the global optimal value is greater than the preset threshold  $C_{\max}$ , the robots consider the global optimal position as the source location and terminate the task. Otherwise, the robots determine that the global optimal position is only a local optimal position and then switch to the plume-finding mode to escape the local extremum area.

The source localization task ends when the robots consider that they have found the source or the number of steps of the robots has reached a preset threshold. The success of the source localization task will be determined by the distance between the source found by the robots and the actual source. If this distance does not exceed the preset threshold  $\Delta d$ , the task is successful (Fig. 2 (c)); otherwise, the task fails.

#### 2.5. Obstacle avoidance algorithm

The same obstacle avoidance algorithm is embedded into both the IPSO and IWOA methods. When a robot calculates that its next position will cross the boundary of a stationary obstacle, the robot will move according to the law of reflection (Fig. 3 (a)). When the robot calculates that it will collide with another robot in the next step, then the robot will move in the opposite direction by a distance  $r \times V_{\max}$  ( $r$  is a random number uniformly distributed in  $[0, 1]$ ) (Fig. 3(b)). More details of the obstacle avoidance algorithm can be found in Ref. [49].

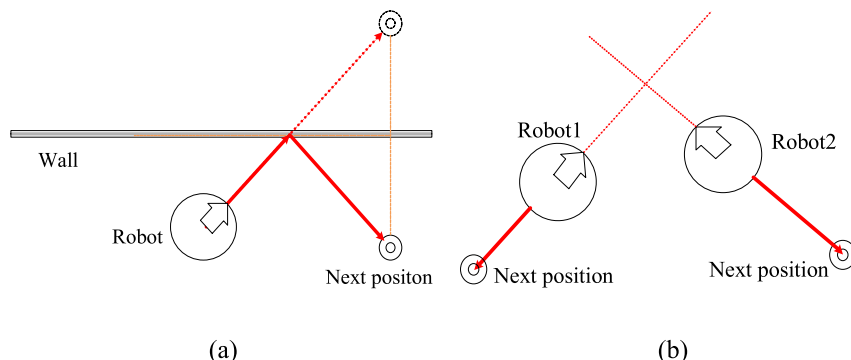


**Fig. 3.** Obstacle avoidance in two situations: (a) collision with the wall; (b) collision with other robots.

### 3. Experimental setup

#### 3.1. Experimental conditions

All experiments were conducted in a laboratory with a length of 6.6 m, width of 4.9 m, and height of 3.3 m (Fig. 4 (a)). The laboratory was divided into an experimental area ( $5.3 \text{ m} \times 4.9 \text{ m}$ ) for conducting the source localization experiments and an operational area ( $1.3 \text{ m} \times 4.9 \text{ m}$ ) for placing a desk, a chair, a cabinet air conditioner (CAC), and a set of tracer-gas release devices (Fig. 4(b)).

To test the IPSO and IWOA methods, we developed an MRO system consisting of three mobile robots with the Kobuki mobile chassis (Yujin Robot, Co., Ltd.). Each robot was equipped with a high-precision laser ranging radar (RPlidar-A1), an industrial personal computer (IPC), an anemometer (Windsonic; response time: 0.25 s; wind speed accuracy:  $\pm 2\%$  at 12 m/s; wind direction accuracy:  $\pm 3\%$  at 12 m/s) and a gas sensor (MICS-5524; response time: 2 s; accuracy:  $\pm 3\%$  at 130 ppm) (Fig. 4(c)).

Ethanol vapor was used as a tracer gas in the experiments [50]; it was generated by heating in a constant temperature water bath at 65 °C and delivered to the source location by using an air pump. By adjusting the release of ethanol vapor through the control devices (Fig. 5(a)), we produced two types of time-varying sources, namely, a periodic source [51] and a decaying source [52] (Fig. 5(b) and (c)).

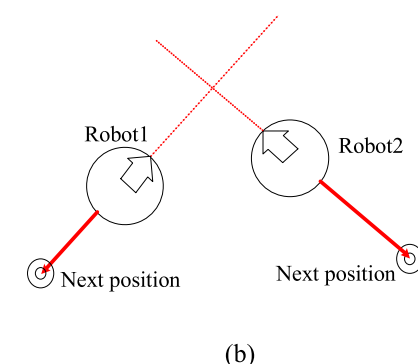
Two source locations, DS and RS, were set in the downwind zone and recirculation zone, respectively, to test the effect of different source locations on the performance of source localization (Fig. 4 (b) and Table 1). Three measuring points, P1, P2 and P3, were set up to monitor the indoor airflow and ethanol concentration (Fig. 4 (b) and Table 1). The two source locations and the three measuring points were all at a height of 1.35 m (the average breathing height of adults in the sitting position [53]).

#### 3.2. Experimental procedure

A total of 160 experiments were conducted to validate and compare the IPSO and IWOA methods. As shown in Fig. 6, these experiments involved a total of 8 scenarios, including two source localization methods (IPSO and IWOA), two time-varying sources (periodic and decaying sources), and two source locations (DS and RS). For each scenario, the experiment was repeated 20 times to obtain statistically significant results.

Before each experiment, all doors and windows were first opened to dilute the residual ethanol vapor. Next, all doors and windows were closed, and the CAC was turned on to create and maintain a steady-state indoor airflow field. Subsequently, the ethanol vapor was released, and after 30 s, the robots started from the starting positions and executed the source localization method autonomously.

Each robot adopted a “move-stop-move” strategy. Specifically, after



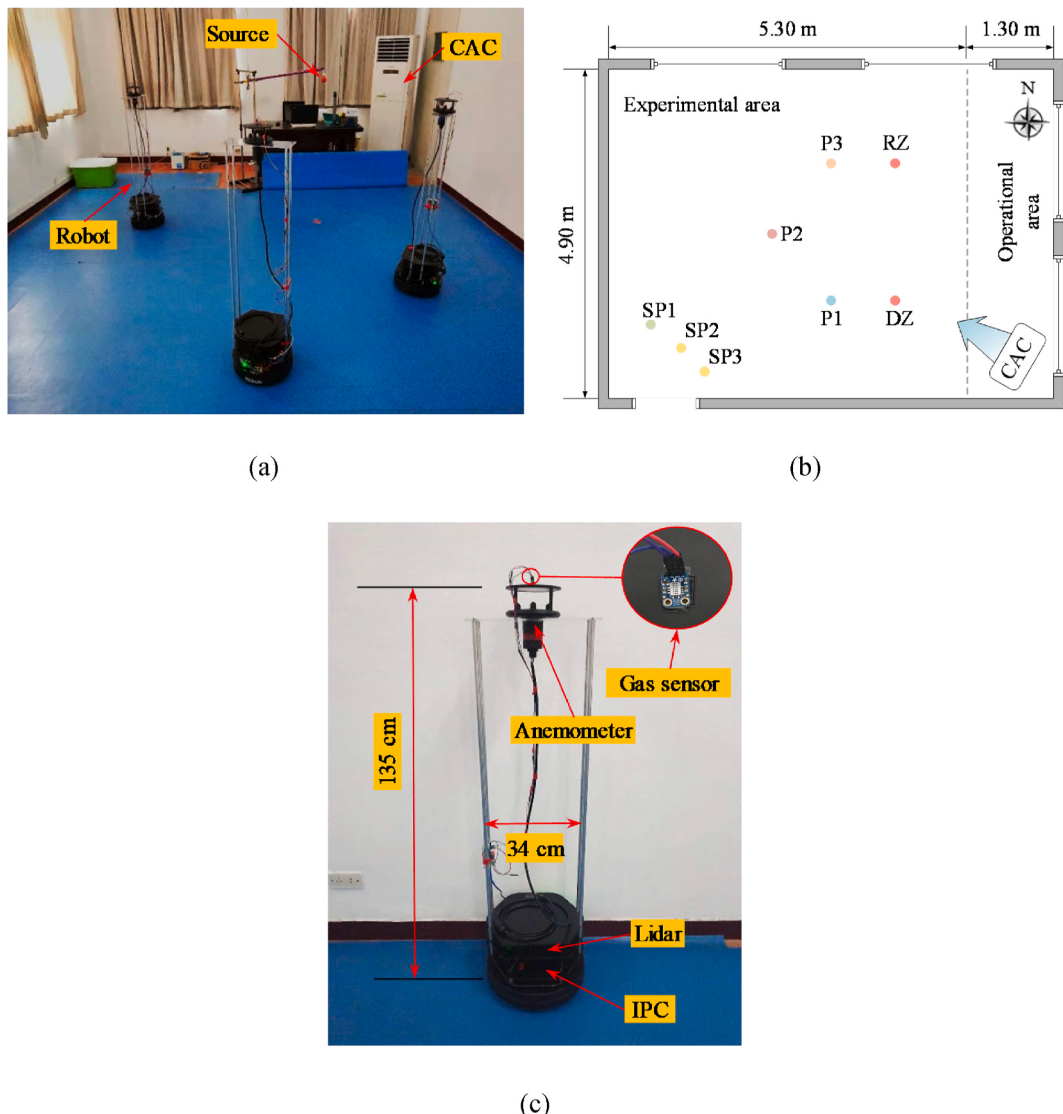


**Fig. 4.** Experimental site and robot: (a) site photo; (b) schematic of the laboratory; (c) configuration of the robot (DS: source location in the downwind zone; RS: source location in the recirculation zone; SP1–SP3: starting positions of the robots; P1–P3: measuring points for airflow and concentration; IPC: industrial personal computer; CAC: cabinet air conditioner).

each robot moved one step, it stayed in place for 6 s to collect airflow and concentration information and then continued to move. The movement speed of each robot was set to 0.3 m/s to achieve a trade-off between reducing the interference to the airflow and concentration fields and improving the efficiency of source localization.

In the experiments, the plume-finding threshold  $C_{\min}$  was 10 ppm, and the source-confirming thresholds  $C_{\max}$  for the periodic and decaying sources were 38 ppm and 65 ppm, respectively. In this study, the source-confirming thresholds were determined by experiments. Before the start of the source localization experiments, 8 sensors were evenly distributed on a circle with a radius of 0.5 m centered on the source, and the concentrations were collected for 300 s after the ethanol vapor was released at an interval of 1 s. The source-confirming threshold is the average of the time-averaged concentrations collected by the 8 sensors in 300 s. If the change in the global optimal position did not exceed 0.4 m (one step of the robots) within 5 consecutive steps, the robots considered that they had become trapped in a local extremum area.

Each robot was allowed to move only up to 50 steps (approximately 15 min) in each experiment to limit the experimental duration. Within 50 steps, if the distance between the source location determined by the robots and the actual source location did not exceed 0.5 m [34], the

experiment was considered successful; otherwise, the experiment was considered to have failed.

## 4. Results and discussion

### 4.1. Airflow and concentration distributions

The airflow velocities and directions collected at three measurement points P1–P3 are shown in Fig. 7 and Table 2. Although the air supply speed and direction of the CAC remained unchanged and all doors and windows were closed to reduce outdoor interference, the airflow velocities and directions at the three measuring points all showed irregular and considerable fluctuations. These results indicate that in a real-world indoor turbulent environment, even if the boundary conditions are deliberately kept unchanged, a steady-state flow field is difficult to achieve.

According to the mean air velocity from high to low in Table 2, the order of the three measuring points is P2, P1, and P3. The results indicate that P2 (at the center of the experimental area) was most affected by the supply airflow, while P3 in the recirculation zone was least affected by the supply airflow. As shown in Fig. 4, P1 was closest to the supply

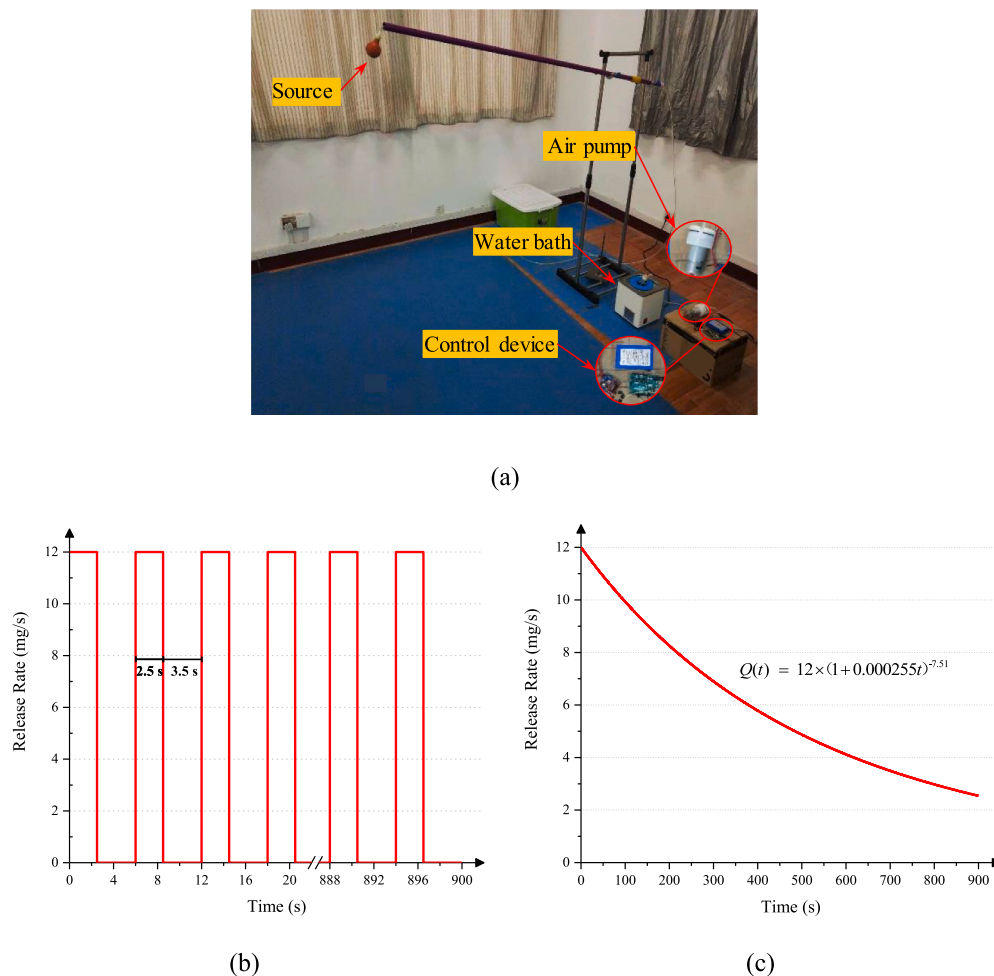


**Fig. 5.** Settings of the ethanol vapor release device: (a) photo; (b) release rate of the periodic source; (c) release rate of the decaying source.

**Table 1**  
Coordinates of the source locations and measuring points.

| Item | Coordinates (m) |      |
|------|-----------------|------|
|      | X               | Y    |
| DS   | 4.20            | 1.70 |
| RS   | 4.20            | 3.50 |
| P1   | 3.80            | 1.70 |
| P2   | 2.75            | 2.45 |
| P3   | 3.80            | 3.50 |

outlet but was less affected by the supply airflow than P2. The reason may be that P1 was farther from the centerline of the supply airflow than P2. According to the fluctuation of the airflow velocity, the three measuring points in descending order is still P2, P1, and P3 (refer to the standard deviation of the airflow velocity in Table 2). The above results indicate that the more each measuring point was affected by the supply airflow, the greater the airflow velocity and the greater the fluctuation of the airflow velocity.

The prevailing airflow directions at the three measuring points were obviously different, and these prevailing airflow directions fluctuated in a relatively large range (Fig. 7 and Table 2). As shown in Fig. 7, the fluctuations of the airflow direction at P1 and P3 were in the range of approximately 180°. The fluctuation range of the airflow direction at P2 was approximately 45°. The reason may be that P2 was closer to the centerline of the supply airflow and was more affected by the supply airflow. In this study, both the IPSO and IWOA algorithms use airflow

information to improve the robot's ability to continuously track the plume, and irregular and large fluctuations in the velocity and direction of the indoor airflow may increase the difficulty of source localization. In addition, the fluctuation of airflow will also increase the difficulty of source localization by further affecting the concentration field.

Fig. 8 shows the curves of the ethanol concentration over time at the three measuring points in the periodic and decaying source scenarios. In both scenarios, the concentrations fluctuated greatly and irregularly. In the periodic source scenario, the fluctuation of the concentration was significantly greater than that in the decaying source scenario, indicating that the concentration at a certain point is affected by both the source and the airflow field. In each scenario, the concentration fluctuation at each measuring point was irregular, and it was quite different from the corresponding release rate curves (Fig. 5). In other words, we cannot directly infer the temporal profile of the source through the concentration curve at each measuring point. This illustrates the complexity of the dispersion of pollutants in turbulent airflow.

According to the results in Fig. 8 and referring to the locations of the measuring points and source in Fig. 4, it can be found that in each scenario, the closer the measuring point was to the source, the greater the concentration fluctuation at that point. In particular, the concentration at P1 has several sharp peaks, which may increase the difficulty of source location. It is worth noting that there were several sharp peaks in the concentration at P1 in each scenario, which may have caused frequent changes in the direction of the concentration gradient and increased the difficulty of source localization.

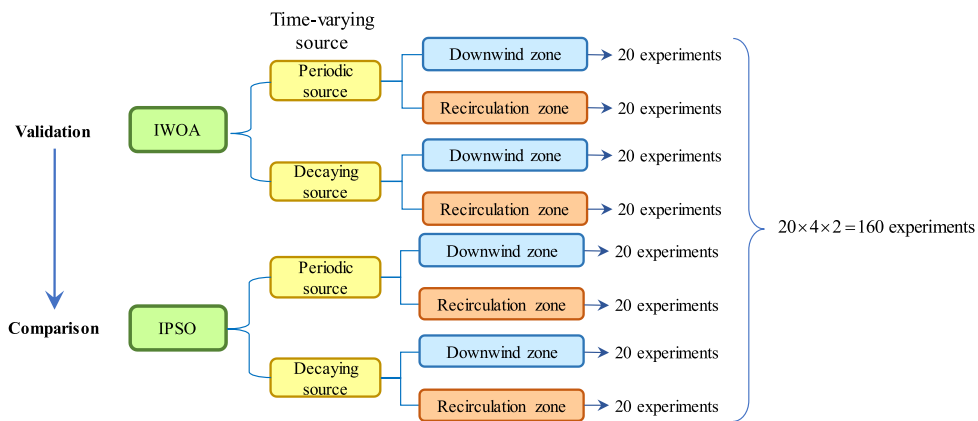


**Fig. 6.** Design of the experimental scenarios.

#### 4.2. Analysis of source localization results

All experimental results of the IPSO and IWOA methods are listed in [Table 3](#). There are four scenarios with two types of time-varying sources (periodic source and decaying source) and two source locations (DS and RS). The pros and cons of the IPSO and IWOA methods were evaluated by three performance indices, namely, the success rate, the mean of the total steps, and the mean distance to the source. The success rate is our most important index because it reflects the applicability of the algorithm to the environment. The latter two indices reflect the efficiency and accuracy of source localization, respectively.

##### 4.2.1. Comparison of the IPSO and IWOA methods

As shown in [Table 3](#), both the IPSO and IWOA methods reached a high success rate in each scenario. For all four scenarios, the mean success rate of the IPSO method was 80%, and that of the IWOA method was 91%. The results indicate that both methods have the potential to locate periodic sources and decaying sources, with the IWOA method being significantly better than the IPSO method in terms of the success rate.

In [Table 4](#), we scored the IPSO and IWOA methods to compare them more intuitively. Each method received 1 point if the success rate was higher, the total number of steps was less, or the distance to the source was closer; otherwise, the method received 0 points. The total scores of the IPSO and IWOA methods for all four scenarios were 4 points and 8 points, respectively, indicating that the IWOA method generally outperformed the IPSO method.

Further analysis of [Table 4](#) shows that the IWOA method won in all four scenarios from the perspective of the success rate and won in three of the four scenarios from the perspective of the mean distance to the source. In contrast, the IWOA method won only in one of the four scenarios from the perspective of the mean of the total steps. These results show that, compared with the IPSO method, the advantage of the IWOA method lies in its success rate and source localization accuracy, while the disadvantage lies in its source localization efficiency.

##### 4.2.2. Effects of the source type and source location

As shown in [Table 3](#), the source type and location have a significant influence on the success rate of the IPSO and IWOA methods, but the influence on the efficiency and accuracy of the two methods is not obvious, and the influence rules are not consistent. Because the success rate is the most concerning, we analyze only the influence of the source type and location on the performance of different methods based on the success rate. In terms of the source type, the success rates of the IPSO and IWOA methods were 83% and 93%, respectively, when locating the decaying source, and the success rates of the IPSO and IWOA methods were 78% and 90%, respectively, when locating the periodic source. In

terms of the source location, the success rates of the IPSO and IWOA methods were 75% and 100%, respectively, when locating the source at DS, and the success rates of the IPSO and IWOA methods were 82.5% and 85%, respectively, when locating the source at RS. The above results show that if only the success rate is considered, both the IPSO and IWOA methods performed better when locating the decaying source and performed better when locating the source at DS. In other words, according to the success rates of the two methods, periodic sources are more difficult to locate than decaying sources, and sources at RS are more difficult to locate than sources at DS.

#### 4.3. Analysis of the source localization process

The experiments in this research involved four scenarios. Due to space limitations, in the following, we discuss only the scenario where the decaying source is located at DS because in this scenario, the results of the IPSO and IWOA methods were quite different. For the scenario where the periodic source is located at DS, the source localization processes of the two methods are provided in Appendix A. The videos of the above mentioned source localization experiments can be found in the supplementary materials.

[Figs. 9 and 10](#) show two successful experiments of the IPSO and IWOA methods to locate the decaying source at DS, respectively. For each method, the robots underwent three processes, namely, plume-finding, plume-tracking, and source-confirming. The IPSO and IWOA methods used different algorithms to track the plume. As shown in [Figs. 9\(a\) and 10\(a\)](#), in the plume-tracking processes, the trajectories of the three robots corresponding to the IPSO and IWOA were obviously different. The robots using the IPSO method mainly moved in the direction of the source location in the plume-tracking process and rarely moved in other directions. In contrast, the robots using the IWOA method were more likely to move in other directions in the plume-tracking process.

Both the IPSO and IWOA methods use the same plume-finding algorithm and source-confirming algorithm. In the following, we take the IWOA method as an example to introduce these two algorithms.

##### (1) Plume-finding algorithm

As shown in [Fig. 10\(a\)](#), after departing from the starting positions, the three robots (R1–R3) began to execute the plume-finding algorithm, which uses a divergent search strategy. The three robots moved in different directions, and their moving trajectories were straight lines and formed two identical angles. At the 6th step, R2 detected a concentration higher than the plume-finding threshold ( $C_{\min}$ ). At this time, the three robots switched to tracking the plume.

In the plume-tracking process, when the robots were trapped in the

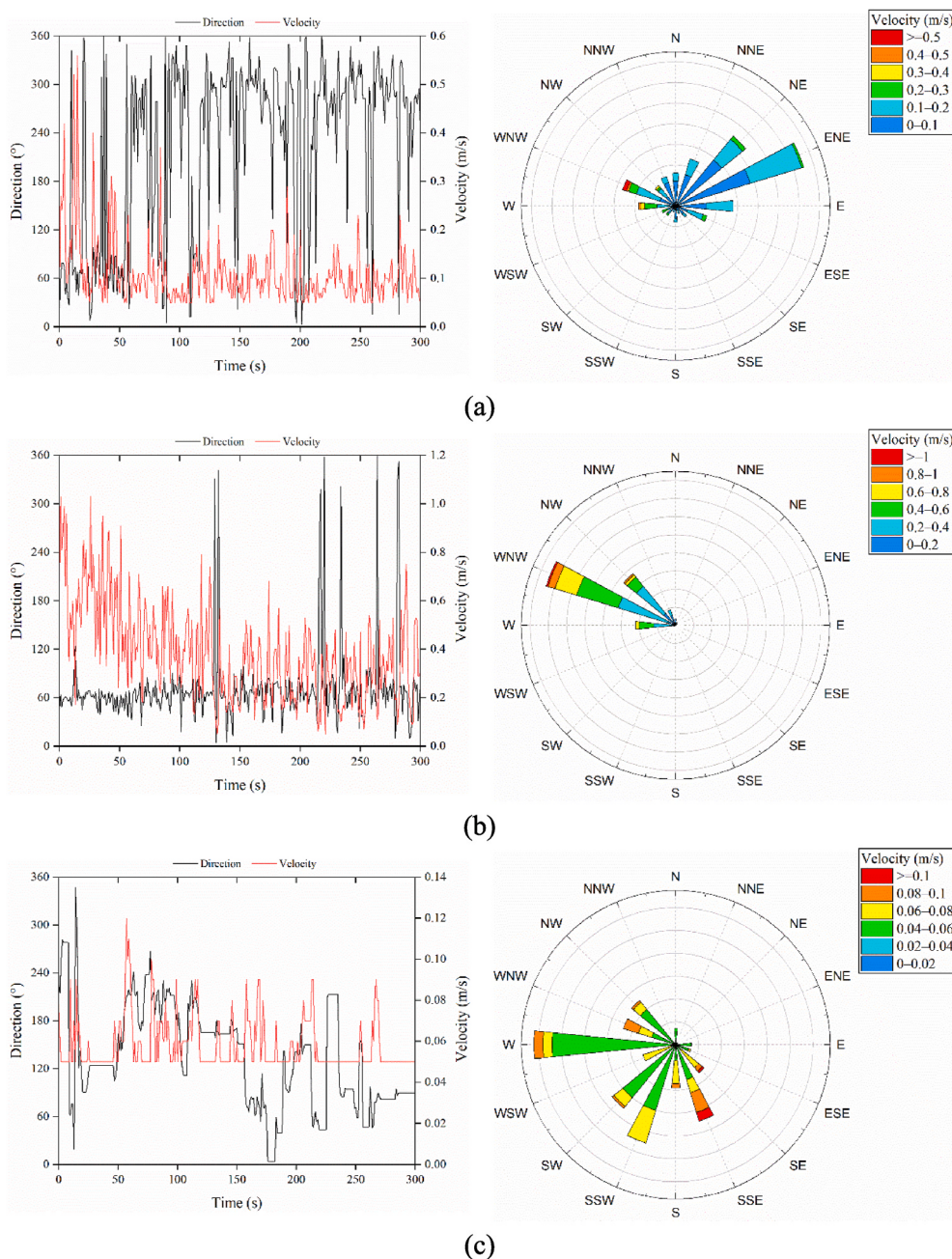


**Fig. 7.** Airflow directions and velocities measured by three ultrasonic anemometers at three measuring points: (a) P1, (b) P2 and (c) P3 (P1–P3: measuring points shown in Fig. 4 (b). The left column shows the line charts, and the right column shows the wind rose charts.).

**Table 2**  
Airflow velocities and directions measured by three ultrasonic anemometers<sup>a</sup>.

| Measuring Points | Airflow velocity (m/s) |                    |      |      | Airflow direction (°) |                    |      |        |
|------------------|------------------------|--------------------|------|------|-----------------------|--------------------|------|--------|
|                  | Mean                   | Standard Deviation | Min  | Max  | Mean                  | Standard Deviation | Min  | Max    |
| P1               | 0.11                   | 0.07               | 0.05 | 0.56 | 222.48                | 110.34             | 2.91 | 360.00 |
| P2               | 0.38                   | 0.20               | 0.05 | 1.03 | 69.82                 | 49.37              | 3.91 | 360.00 |
| P3               | 0.06                   | 0.01               | 0.05 | 0.12 | 134.03                | 64.62              | 3.91 | 347.08 |

<sup>a</sup> The measuring points P1–P3 are shown in Fig. 4 (b). P2 is located at the center of the experimental area, and P1 and P3 are located in the downwind zone and the recirculation zone, respectively.

local extremum area, they triggered the plume-finding algorithm to escape the area. As shown in Fig. 10, because the global optimal position had not changed from the 18th to 22nd step (5 consecutive steps), R2 made a judgment that it was trapped in the local extremum area. At the

22nd step, the robots used the plume-finding algorithm to escape the local extremum area and tried to find a higher concentration.

## (2) Source-confirming algorithm

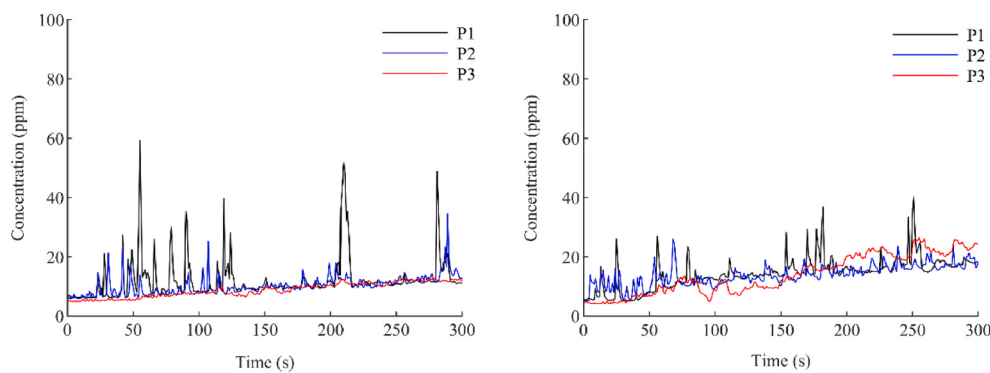


**Fig. 8.** Concentrations measured in the scenarios with (a) a periodic source and (b) a decaying source (P1–P3: measuring points; ethanol vapor released at DS, as shown in Fig. 4 (b)).

**Table 3**  
Source localization results of the IPSO and IWOA methods.

| Method                   | Source type     | Source location | Number of successful experiments <sup>a</sup> | Success rate | Mean of total steps | Mean distance to source (m) |
|--------------------------|-----------------|-----------------|---|--------------|---------------------|-----------------------------|
| IPSO                     | Periodic source | DS              | 17  | 85%          | 24.5                | 0.26                        |
|                          |                 | RS              | 14  | 70%          | 29.2                | 0.33                        |
|                          |                 | Mean            | 15.5  | 78%          | 26.9                | 0.30                        |
|                          | Decaying source | DS              | 17  | 85%          | 20.7                | 0.18                        |
|                          |                 | RS              | 16  | 80%          | 25.9                | 0.27                        |
|                          |                 | Mean            | 16.5  | 83%          | 23.3                | 0.23                        |
| Mean for the IPSO method |                 | 16.0            |   | 80%          | 25.1                | 0.26                        |
| IWOA                     | Periodic source | DS              | 20  | 100%         | 25.3                | 0.16                        |
|                          |                 | RS              | 16  | 80%          | 28.8                | 0.23                        |
|                          |                 | Mean            | 18.0  | 90%          | 27.1                | 0.20                        |
|                          | Decaying source | DS              | 20  | 100%         | 27.7                | 0.25                        |
|                          |                 | RS              | 17  | 85%          | 29.1                | 0.24                        |
|                          |                 | Mean            | 18.5  | 93%          | 28.4                | 0.25                        |
| Mean for the IWOA method |                 | 18.3            |   | 91%          | 27.7                | 0.22                        |

<sup>a</sup> 20 experiments were conducted for each scenario.

**Table 4**  
Performance scores of the IPSO and IWOA methods.

| Source type     | Source location | Success rate |      | Mean of the total steps |      | Mean distance to the source |      |
|-----------------|-----------------|--------------|------|-------------------------|------|-----------------------------|------|
|                 |                 | IPSO         | IWOA | IPSO                    | IWOA | IPSO                        | IWOA |
| Periodic source | DS              | 0            | 1    | 1                       | 0    | 0                           | 1    |
|                 | RS              | 0            | 1    | 0                       | 1    | 0                           | 1    |
|                 | Subtotal        | 0            | 2    | 1                       | 1    | 0                           | 2    |
| Decaying source | DS              | 0            | 1    | 1                       | 0    | 1                           | 0    |
|                 | RS              | 0            | 1    | 1                       | 0    | 0                           | 1    |
|                 | Subtotal        | 0            | 2    | 2                       | 0    | 1                           | 1    |
| Total           |                 | 0            | 4    | 3                       | 1    | 1                           | 3    |

The robots confirm the source by comparing the concentration at the global optimal position and the source confirmation threshold ( $C_{\max}$ ). As shown in Fig. 10(b), at the 23rd step, R2 detected a concentration higher than  $C_{\max}$ , and the three robots did not detect a higher concentration in the next 5 steps (24th to 28th step); thus, the source-confirming algorithm determined that the source had been successfully located and ended the source localization process. The distance between the source location determined by the robots and the actual source location was 0.21 m (less than 0.5 m). Therefore, this source localization experiment was considered to be successful.

#### 4.4. Limitations and future study

To validate and compare the IPSO and IWOA methods in locating indoor time-varying sources, we conducted a total of 160 independent experiments, which far exceed the workload of related studies that have been published [44,54–58]. Nevertheless, due to the time-consuming

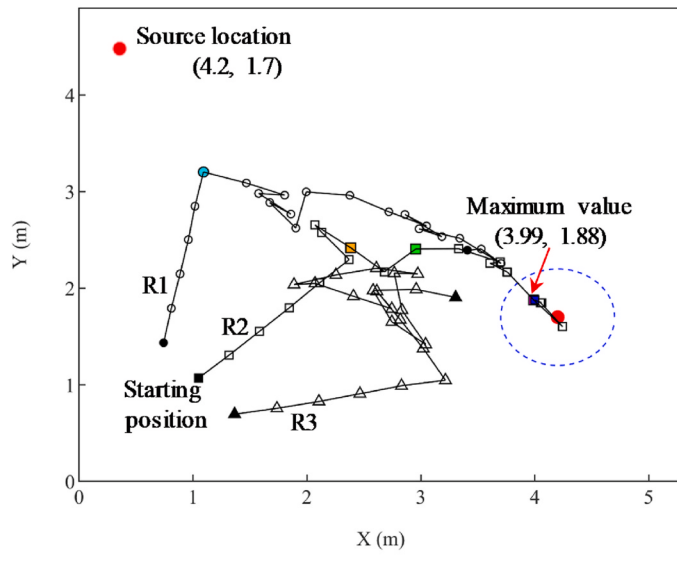
and laborious nature of experimental study, this study still cannot fully consider a variety of influencing factors, such as airflow velocity, gas type, starting position, starting angle of motion, robot motion speed, sensor accuracy, etc. Therefore, the findings or results of this study may be controversial for different application scenarios. In future study, we will consider combining experimental and numerical methods to test more influencing factors and scenarios.

In this study, the robots determine whether the real source is found by comparing the global optimal value with a preset threshold  $C_{\max}$ . How to determine a reasonable concentration threshold in practical applications is both critical and difficult. To the best of our knowledge, this problem has not been properly resolved in the international academic community. To date, many related studies determined the concentration threshold through numerical simulation of a specific application scenario [59,60]. In this study, we determined this threshold by conducting the experiments described in Section 3.2 in advance. For practical applications, we recommend that before the robots are put into use, experimental or numerical experiments should be conducted according to specific application scenarios to determine a source-confirming threshold. In addition, in future study, we will study the use of robot vision as an auxiliary means to determine whether there is a source after the robots entered a local extremum area.

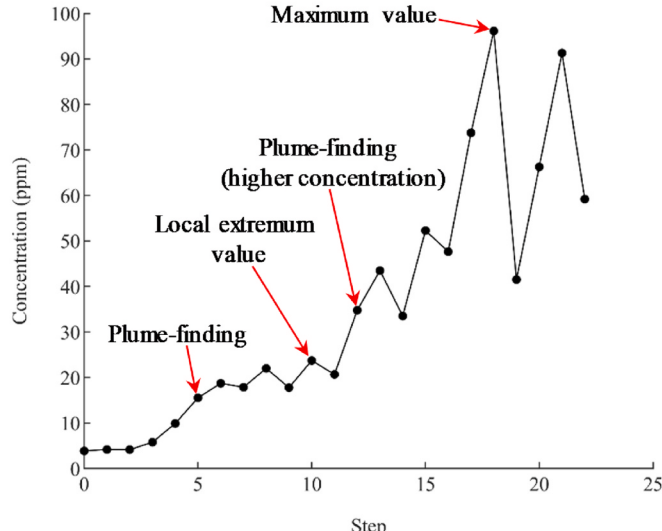
#### 5. Conclusions

To locate a time-varying source in an indoor ventilated environment, we designed and developed a source localization system composed of three robots and compiled the IPSO and IWOA methods we proposed previously into programs that can be executed by the system. A total of 160 experiments were conducted in four experimental scenarios

- Plume-finding (5<sup>th</sup> step)
- Plume-finding (higher concentration) (12<sup>th</sup> step)
- Final source declaration (22<sup>nd</sup> step)
- Trapping in a local extremum area (10<sup>th</sup> step)
- Source-confirming (18<sup>th</sup> step)



(a)



(b)

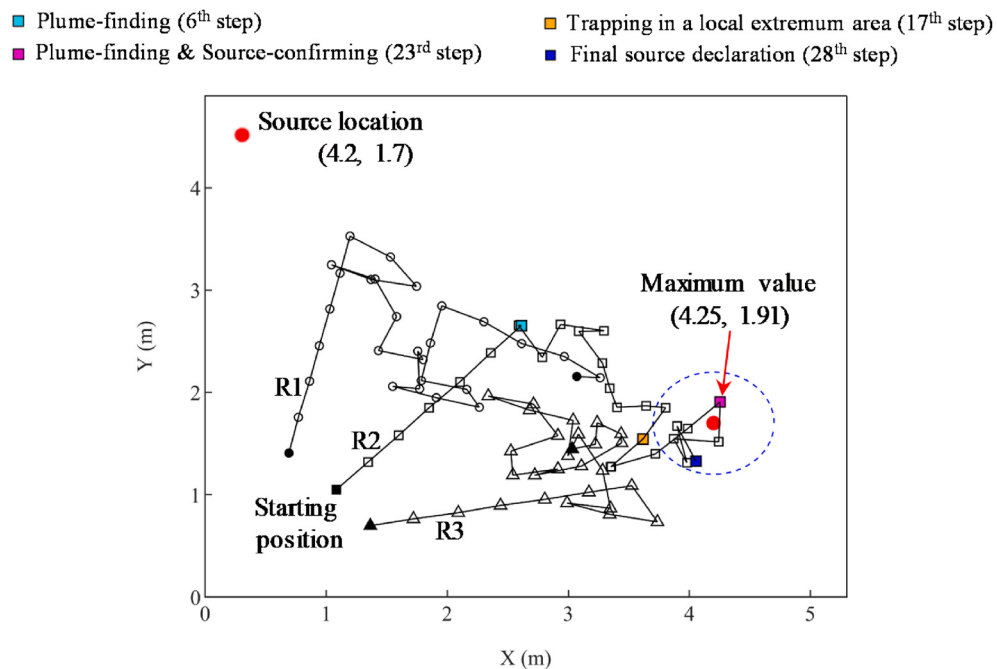
**Fig. 9.** A successful experiment in which the IPSO method is used to locate a decaying source at DS: (a) trajectories of robots R1–R3; (b) maximum time-averaged concentration collected by R1–R3 at each step.

(combinations of two time-varying sources and two source locations) to validate and compare the IPSO and IWOA methods. The experimental results lead to the following conclusions:

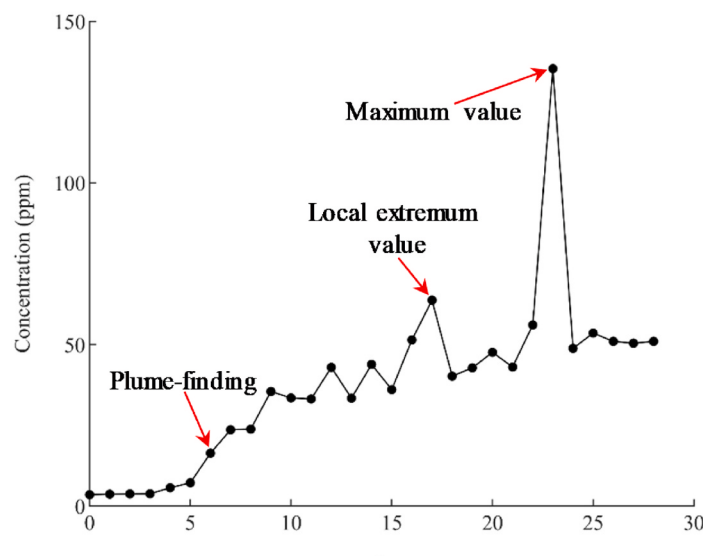
- (1) In the experiments, although all doors and windows were closed and the air supply status of CAC remained unchanged, irregular fluctuations of airflow and concentration were observed, which will increase the difficulty of robotic source localization.
- (2) For all four scenarios, the average success rates of the IPSO and IWOA methods were 80% and 91%, respectively, which indicate that the two methods have the potential to locate time-varying

sources in indoor ventilated environments. In addition, the IWOA method generally outperformed the IPSO method. The advantage of the IWOA method lies in the success rate and locating accuracy, while its disadvantage lies in the locating efficiency.

- (3) The success rates of the IPSO and IWOA methods were both significantly affected by source type and source location. From the perspective of success rate, the two methods were more difficult to locate the periodic source than the decaying source, and were more difficult to locate the source at RS than that at DS.



(a)



(b)

**Fig. 10.** A successful experiment in which the IWOA method is used to locate a decaying source at DS: (a) trajectories of robots R1–R3; (b) maximum time-averaged concentration collected by R1–R3 at each step.

- (4) The trajectories of the robots show that compared with the IPSO method, the plume-tracking strategy of the IWOA method will expand the search range of the robots, thereby improving the success rate and accuracy of source localization. However, this strategy will also increase the steps of source localization and sacrifice locating efficiency.

#### Declaration of competing interest

The authors declare that they have no known competing financial

interests or personal relationships that could have appeared to influence the work reported in this paper.

#### Acknowledgements

This study was supported by the National Natural Science Foundation of China (Grant No. 51478468) and the National Natural Science Foundation of China (Grant No. 51708286).

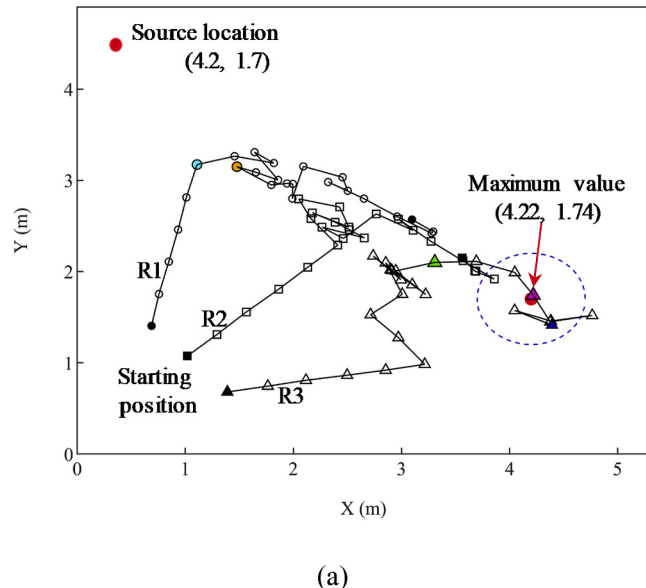
## Appendix B. Supplementary data

Supplementary data to this article can be found online at <https://doi.org/10.1016/j.buildenv.2021.108560>.

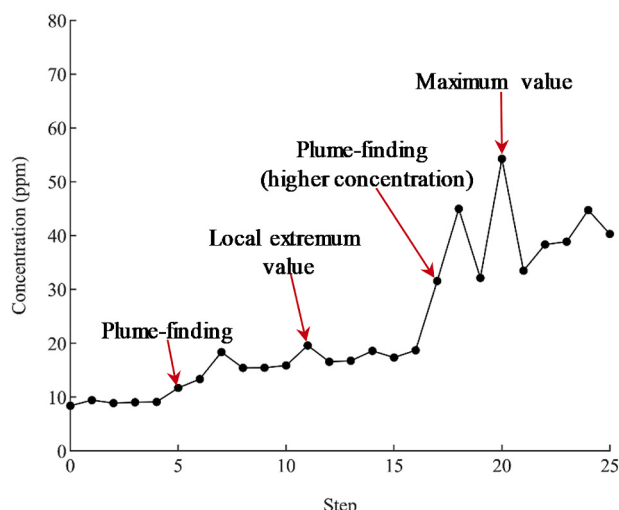
## Appendix A. Source localization processes of the IPSO and IWOA methods in locating a periodic source at DS

Figs. A1 and A2 show the source localization processes of robots R1–R3 using the IPSO and IWOA methods, respectively, to locate a periodic source at DS.

- Plume-finding (5<sup>th</sup> step)
- Trapping in a local extremum area (11<sup>th</sup> step)
- ▲ Plume-finding (higher concentration) (17<sup>th</sup> step)
- ▲ Source-confirming (20<sup>th</sup> step)
- ▲ Final source declaration (25<sup>th</sup> step)



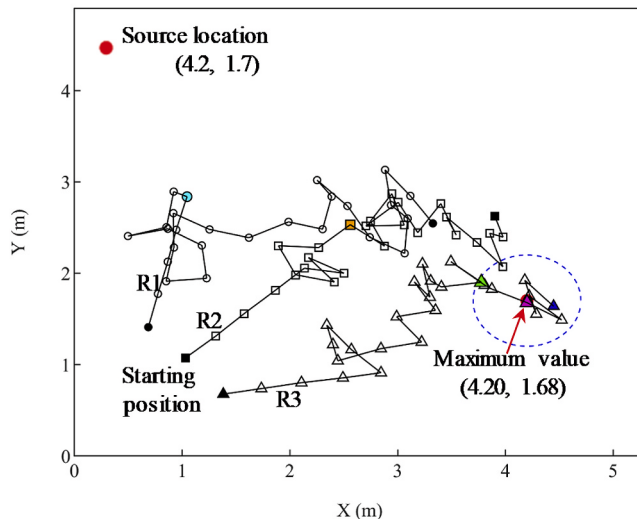
(a)



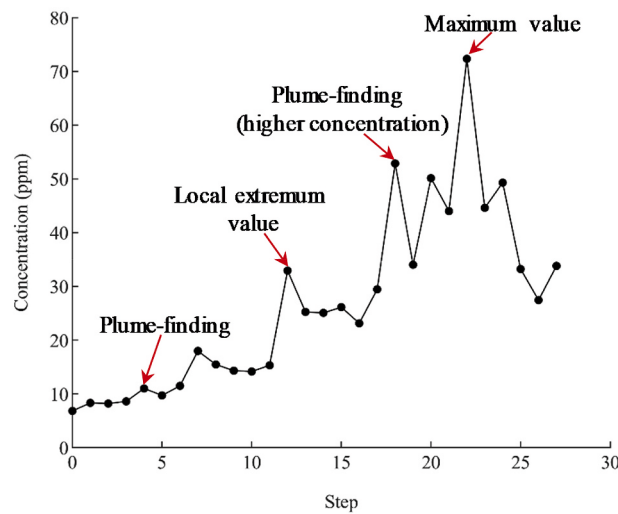
(b)

**Fig. A1.** A successful experiment in which the IPSO method is used to locate a periodic source at DS: (a) trajectories of robots R1–R3; (b) maximum time-averaged concentration collected by R1–R3 at each step.

- Plume-finding (4<sup>th</sup> step)
- Trapping in a local extremum area (12<sup>th</sup> step)
- ▲ Plume-finding (higher concentration) (18<sup>th</sup> step)
- ▲ Source-confirming (22<sup>nd</sup> step)
- ▲ Final source declaration (27<sup>th</sup> step)



(a)



(b)

**Fig. A2.** A successful experiment in which the IWOA method is used to locate a periodic source at DS: (a) trajectories of robots R1–R3; (b) maximum time-averaged concentration collected by R1–R3 at each step.

## References

- [1] X. Li, H. Cai, L. Zhao, *Antiterrorist Emergency Ventilation: System, Strategy and Decision-Making*, Nova Science Publishers, 2009.
- [2] L. Zeng, J. Gao, L. Lv, R. Zhang, Y. Chen, X. Zhang, Z. Huang, Z. Zhang, Markov-chain-based inverse modeling to fast localize hazardous gaseous pollutant sources in buildings with ventilation systems, *Build. Environ.* 169 (2020) 106584, <https://doi.org/10.1016/j.buildenv.2019.106584>.
- [3] Y. Zhao, B. Chen, Z. Zhu, F. Chen, Y. Wang, Y. Ji, Searching the diffusive source in an unknown obstructed environment by cognitive strategies with forbidden areas, *Build. Environ.* 186 (2020) 107349, <https://doi.org/10.1016/j.buildenv.2020.107349>.
- [4] Z. Li, Z.F. Tian, T. Lu, H. Wang, Assessment of different plume-tracing algorithms for indoor plumes, *Build. Environ.* 173 (2020) 106746, <https://doi.org/10.1016/j.buildenv.2020.106746>.
- [5] Z. (John) Zhai, X. Liu, H. Wang, Y. Li, J. Liu, Experimental verification of tracking algorithm for dynamically-releasing single indoor contaminant, *Build. Simul.* 5 (2012) 5–14, <https://doi.org/10.1007/s12273-011-0041-8>.
- [6] X. Chen, J. Huang, Odor source localization algorithms on mobile robots: a review and future outlook, *Robot. Autonom. Syst.* 112 (2019) 123–136, <https://doi.org/10.1016/j.robot.2018.11.014>.
- [7] M. Day, Covid-19: identifying and isolating asymptomatic people helped eliminate virus in Italian village, *BMJ Br. Med. J. (Clin. Res. Ed.)* 368 (2020), <https://doi.org/10.1136/bmj.m1165>.
- [8] Y. Fan, K. Kameishi, S. Onishi, K. Ito, Field-based study on the energy-saving effects of CO<sub>2</sub> demand controlled ventilation in an office with application of Energy recovery ventilators, *Energy Build.* 68 (2014) 412–422, <https://doi.org/10.1016/j.enbuild.2013.09.043>.
- [9] R. Barber, M.A. Rodriguez-Conejo, J. Melendez, S. Garrido, Design of an infrared imaging system for robotic inspection of gas leaks in industrial environments, *Int. J. Adv. Rob. Syst.* 12 (2015) 23, <https://doi.org/10.5772/60058>.

- [10] F. Li, H. Cai, J. Xu, K. Zhang, Q. Feng, H. Wang, Gas distribution mapping for indoor environments based on laser absorption spectroscopy: development of an improved tomographic algorithm, *Build. Environ.* 172 (2020) 106724, <https://doi.org/10.1016/j.buildenv.2020.106724>.
- [11] L. Zeng, J. Gao, B. Du, R. Zhang, X. Zhang, Probability-based inverse characterization of the instantaneous pollutant source within a ventilation system, *Build. Environ.* 143 (2018) 378–389, <https://doi.org/10.1016/j.buildenv.2018.07.036>.
- [12] J. Gao, L. Zeng, L. Wu, X. Ding, X. Zhang, Solution for sudden contamination transport through air duct system: under a puff release, *Build. Environ.* 100 (2016) 19–27, <https://doi.org/10.1016/j.buildenv.2016.01.024>.
- [13] A. Bastani, F. Haghighat, J.A. Kozinski, Contaminant source identification within a building: toward design of immune buildings, *Build. Environ.* 51 (2012) 320–329, <https://doi.org/10.1016/j.buildenv.2011.12.002>.
- [14] Q.-H. Meng, W.-X. Yang, Y. Wang, F. Li, M. Zeng, Adapting an ant colony metaphor for multi-robot chemical plume tracing, *Sensors* 12 (2012) 4737–4763, <https://doi.org/10.3390/s12040473>.
- [15] X. Shao, X. Li, H. Ma, Identification of constant contaminant sources in a test chamber with real sensors, *Indoor Built Environ.* 25 (2016) 997–1010, <https://doi.org/10.1177/1420326X15604673>.
- [16] H. Wang, S. Lu, J. Cheng, Z. (John) Zhai, Inverse modeling of indoor instantaneous airborne contaminant source location with adjoint probability-based method under dynamic airflow field, *Build. Environ.* 117 (2017) 178–190, <https://doi.org/10.1016/j.buildenv.2017.03.017>.
- [17] Y. Yang, Q. Feng, H. Cai, J. Xu, F. Li, Z. Deng, C. Yan, X. Li, Experimental study on three single-robot active olfaction algorithms for locating contaminant sources in indoor environments with no strong airflow, *Build. Environ.* 155 (2019) 320–333, <https://doi.org/10.1016/j.buildenv.2019.03.043>.
- [18] T. (Tim) Zhang, S. Yin, S. Wang, An inverse method based on CFD to quantify the temporal release rate of a continuously released pollutant source, *Atmos. Environ.* 77 (2013) 62–77, <https://doi.org/10.1016/j.atmosenv.2013.04.057>.
- [19] Y. Wei, H. Zhou, T. (Tim) Zhang, S. Wang, Inverse identification of multiple temporal sources releasing the same tracer gaseous pollutant, *Build. Environ.* 118 (2017) 184–195, <https://doi.org/10.1016/j.buildenv.2017.03.026>.
- [20] X. Liu, Z. (John) Zhai, Inverse modeling methods for indoor airborne pollutant tracking: literature review and fundamentals, *Indoor Air* 17 (2007) 419–438, <https://doi.org/10.1111/j.1600-0668.2007.00497.x>.
- [21] D. Liu, F.-Y. Zhao, H.-Q. Wang, E. Rank, History source identification of airborne pollutant dispersions in a slot ventilated building enclosure, *Int. J. Therm. Sci.* 64 (2013) 81–92, <https://doi.org/10.1016/j.ijthermalsci.2012.08.005>.
- [22] T. (Tim) Zhang, Q. Chen, Identification of contaminant sources in enclosed environments by inverse CFD modeling, *Indoor Air* 17 (2007) 167–177, <https://doi.org/10.1111/j.1600-0668.2006.00452.x>.
- [23] T. (Tim) Zhang, Q. Chen, Identification of contaminant sources in enclosed spaces by a single sensor, *Indoor Air* 17 (2007) 439–449.
- [24] V. Akçelik, G. Biroš, O. Ghattas, K.R. Long, B. van B. Waanders, A variational finite element method for source inversion for convective-diffusive transport, *Finite Elem. Anal. Des.* 39 (2003) 683–705, [https://doi.org/10.1016/s0168-874x\(03\)00054-4](https://doi.org/10.1016/s0168-874x(03)00054-4).
- [25] X. Liu, Z. (John) Zhai, Location identification for indoor instantaneous point contaminant source by probability-based inverse Computational Fluid Dynamics modeling, *Indoor Air* 18 (2008) 2–11, <https://doi.org/10.1111/j.1600-0668.2007.00499.x>.
- [26] F. Li, X. Liu, J. Liu, H. Cai, H. Wang, K. Zhang, C. Dai, Solutions to mitigate the impact of measurement noise on the air pollution source strength estimation in a multi-zone building, *Build. Simul.* 13 (2020) 1329–1337, <https://doi.org/10.1007/s12273-020-0635-0>.
- [27] H. Cai, X. Li, Z. Chen, M. Wang, Rapid identification of multiple constantly-released contaminant sources in indoor environments with unknown release time, *Build. Environ.* 81 (2014) 7–19, <https://doi.org/10.1016/j.buildenv.2014.06.006>.
- [28] H. Cai, X. Li, Z. Chen, L. Kong, Fast identification of multiple indoor constant contaminant sources by ideal sensors: a theoretical model and numerical validation, *Indoor Built Environ.* 22 (2013) 897–909, <https://doi.org/10.1177/1420326X12463584>.
- [29] P. Sreedharan, M.D. Sohn, A.J. Gadgil, W.W. Nazaroff, Systems approach to evaluating sensor characteristics for real-time monitoring of high-risk indoor contaminant releases, *Atmos. Environ.* 40 (2006) 3490–3502, <https://doi.org/10.1016/j.atmosenv.2006.01.052>.
- [30] P. Sreedharan, M.D. Sohn, W.W. Nazaroff, A.J. Gadgil, Influence of indoor transport and mixing time scales on the performance of sensor systems for characterizing contaminant releases, *Atmos. Environ.* 41 (2007) 9530–9542, <https://doi.org/10.1016/j.atmosenv.2007.08.039>.
- [31] T. (Tim) Zhang, H. Zhou, S. Wang, Inverse identification of the release location, temporal rates, and sensor alarming time of an airborne pollutant source, *Indoor Air* 25 (2015) 415–427, <https://doi.org/10.1111/ina.12153>.
- [32] A.T. Hayes, A. Martinoli, R.M. Goodman, Distributed odor source localization, *IEEE Sensor. J.* 2 (2002) 260–271, <https://doi.org/10.1109/JSEN.2002.800682>.
- [33] H. Ishida, Y. Wada, H. Matsukura, Chemical sensing in robotic applications: a review, *IEEE Sensor. J.* 12 (2012) 3163–3173, <https://doi.org/10.1109/JSEN.2012.2208740>.
- [34] J.-G. Li, Q.-H. Meng, Y. Wang, M. Zeng, Odor source localization using a mobile robot in outdoor airflow environments with a particle filter algorithm, *Aut. Robots* 30 (2011) 281–292, <https://doi.org/10.1007/s10514-011-9219-2>.
- [35] Y. Zhao, B. Chen, Z. Zhu, F. Chen, Y. Wang, Y. Ji, Searching the diffusive source in an unknown obstructed environment by cognitive strategies with forbidden areas, *Build. Environ.* 186 (2020) 107349, <https://doi.org/10.1016/j.buildenv.2020.107349>.
- [36] Q. Feng, H. Cai, F. Li, X. Liu, S. Liu, J. Xu, An improved particle swarm optimization method for locating time-varying indoor particle sources, *Build. Environ.* 147 (2019) 146–157, <https://doi.org/10.1016/j.buildenv.2018.10.008>.
- [37] H. Ishida, T. Nakamoto, T. Morizumi, Gas/odor plume tracing robot, *Sensor. Update* 6 (1999) 397–418, [https://doi.org/10.1002/1616-8984\(199911\)6:1<397::AID-SEUP397>3.0.CO;2-3](https://doi.org/10.1002/1616-8984(199911)6:1<397::AID-SEUP397>3.0.CO;2-3).
- [38] Y. Chen, H. Cai, Z. Chen, Q. Feng, Using multi-robot active olfaction method to locate time-varying contaminant source in indoor environment, *Build. Environ.* 118 (2017) 101–112, <https://doi.org/10.1016/j.buildenv.2017.03.030>.
- [39] Q. Feng, H. Cai, F. Li, Y. Yang, Z. Chen, Locating time-varying contaminant sources in 3D indoor environments with three typical ventilation systems using a multi-robot active olfaction method, *Build. Simul.* 11 (2018) 597–611, <https://doi.org/10.1007/s12273-017-0424-6>.
- [40] Y. Yang, B. Zhang, Q. Feng, H. Cai, M. Jiang, K. Zhou, F. Li, S. Liu, X. Li, Towards locating time-varying indoor particle sources: development of two multi-robot olfaction methods based on whale optimization algorithm, *Build. Environ.* 166 (2019) 106413, <https://doi.org/10.1016/j.buildenv.2019.106413>.
- [41] T.L. Payne, M.C. Birch, Mechanisms in Insect Olfaction, 1986.
- [42] Q. Feng, C. Zhang, J. Lu, H. Cai, Z. Chen, Y. Yang, F. Li, X. Li, Source localization in dynamic indoor environments with natural ventilation: an experimental study of a particle swarm optimization-based multi-robot olfaction method, *Build. Environ.* 161 (2019) 106228, <https://doi.org/10.1016/j.buildenv.2019.106228>.
- [43] G. Kowadlo, R.A. Russell, Robot odor localization: a taxonomy and survey, *Int. J. Robot. Res.* 27 (2008) 869–894, <https://doi.org/10.1177/0278364908095118>.
- [44] X. Chen, J. Huang, Combining particle filter algorithm with bio-inspired anemotaxis behavior: a smoke plume tracking method and its robotic experiment validation, *Measurement* 154 (2020) 107482, <https://doi.org/10.1016/j.measurement.2020.107482>.
- [45] M. Dadgar, S. Jafari, A. Hamzeh, A PSO-based multi-robot cooperation method for target searching in unknown environments, *Neurocomputing* 177 (2016) 62–74, <https://doi.org/10.1016/j.neucom.2015.11.007>.
- [46] Q. Feng, H. Cai, Y. Yang, J. Xu, M. Jiang, F. Li, X. Li, C. Yan, An experimental and numerical study on a multi-robot source localization method independent of airflow information in dynamic indoor environments, *Sustain. Cities. Soc.* 53 (2020) 101897, <https://doi.org/10.1016/j.scs.2019.101897>.
- [47] S. Mirjalili, A. Lewis, The whale optimization algorithm, *Adv. Eng. Software* 95 (2016) 51–67, <https://doi.org/10.1016/j.advengsoft.2016.01.008>.
- [48] Q. Feng, H. Cai, F. Li, X. Liu, S. Liu, J. Xu, An improved particle swarm optimization method for locating time-varying indoor particle sources, *Build. Environ.* 147 (2019) 146–157, <https://doi.org/10.1016/j.buildenv.2018.10.008>.
- [49] Q. Feng, H. Cai, Z. Chen, Y. Yang, J. Lu, F. Li, J. Xu, X. Li, Experimental study on a comprehensive particle swarm optimization method for locating contaminant sources in dynamic indoor environments with mechanical ventilation, *Energy Build.* 196 (2019) 145–156, <https://doi.org/10.1016/j.enbuild.2019.03.032>.
- [50] K. Kamarudin, A.Y.M. Shakaff, V.H. Bennetts, S.M. Mamduh, A. Zakaria, R. Visvanathan, A.S.A. Yeon, L.M. Kamarudin, Integrating SLAM and gas distribution mapping (SLAM-GDM) for real-time gas source localization, *Adv. Robot.* 32 (2018) 903–917, <https://doi.org/10.1080/01691864.2018.1516568>.
- [51] S. Zhu, S. Kato, S. Murakami, T. Hayashi, Study on inhalation region by means of CFD analysis and experiment, *Build. Environ.* 40 (2005) 1329–1336, <https://doi.org/10.1016/j.buildenv.2004.11.009>.
- [52] V.H.Y. Tam, R.B. Higgins, Simple transient release rate models for releases of pressurised liquid petroleum gas from pipelines, *J. Hazard Mater.* 25 (1990) 193–203, [https://doi.org/10.1016/0304-3894\(90\)85078-h](https://doi.org/10.1016/0304-3894(90)85078-h).
- [53] L. Morawska, A. Afshari, G.N. Bae, G. Buonanno, C.Y.H. Chao, O. Hänninen, W. Hofmann, C. Isaxon, E.R. Jayaratne, P. Pasanen, T. Saltherammer, M. Waring, A. Wierzbicka, Indoor aerosols: from personal exposure to risk assessment, *Indoor Air* 23 (2013) 462–487, <https://doi.org/10.1111/ina.12044>.
- [54] J. Lee, S. Park, E.T. Matson, Circular Movement Algorithm for Gas Tracking in Indoor Environment, 2016 IEEE Int. Conf. Syst. Man Cybern. SMC, 2016, <https://doi.org/10.1109/SMC.2016.7844871>, 004082–004087.
- [55] W. Jatmiko, F. Jovan, R.Y.S. Dhiemans, M.S. Alvissalim, A. Febrian, D. Widiyanto, D.M.J. Purnomo, H.A. Wisesa, T. Fukuda, K. Sekiyama, PSO algorithm for single and multiple odor sources localization problems: progress and challenge, *Int. J. Smart Sens. Intell. Syst.* 9 (2016), <https://doi.org/10.21307/ijssis-2017-925>.
- [56] Q.-H. Meng, W.X. Yang, Y. Wang, M. Zeng, Collective odor source estimation and search in time-variant airflow environments using mobile robots, *Sensors* 11 (2011) 10415–10443, <https://doi.org/10.3390/s111110415>.
- [57] W. Jatmiko, F. Jovan, R.Y.S. Dhiemans, A.M. Sakti, F.M. Ivan, A. Febrian, T. Fukuda, K. Sekiyama, Robots implementation for odor source localization using PSO algorithm, *WSEAS Trans. Circuits Syst.* 10 (2011) 115–125.
- [58] H. Ishida, H. Tanaka, H. Taniguchi, T. Morizumi, Mobile robot navigation using vision and olfaction to search for a gas/odor source, *Aut. Robots* 20 (2006) 231–238, <https://doi.org/10.1007/s10514-006-7100-5>.
- [59] W. Jatmiko, K. Sekiyama, T. Fukuda, A PSO-based mobile robot for odor source localization in dynamic advection-diffusion with obstacles environment: theory, simulation and measurement, *IEEE Comput. Intell. Mag.* 2 (2007) 37–51, <https://doi.org/10.1109/mci.2007.353419>.
- [60] M. Awadalla, T.F. Lu, Z.F. Tian, B. Dally, Z.Z. Liu, 3D framework combining CFD and MATLAB techniques for plume source localization research, *Build. Environ.* 70 (2013) 10–19, <https://doi.org/10.1016/j.buildenv.2013.07.021>.